Available online at www.sciencedirect.com

ScienceDirect

Current Opinion in Electrochemistry

Review Article

Advancements in hydrogen production using alkaline electrolysis systems: A short review on experimental and simulation studies

Lucía Paula Campo Schneider[1,a], Maryem Dhrioua[1,a], Dirk Ullmer[1], Franz Egert[1,2], Hans Julian Wiggenhauser[1], Kamal Ghotia[1], Nicolas Kawerau[1], Davide Grilli[1], Fatemeh Razmjooei[1] and Syed Asif Ansar[1]

Abstract

Although alkaline water electrolysis (AWE) is a highly mature technology for hydrogen production, its potential is hindered by relatively low efficiencies at high current densities. On the other hand, to conform with "RePowerEU" directives, coupling electrolyzers with new renewable energy sources (RES) is highly demanded. However, integrating fluctuating RES poses challenges for the AWE due to increasing gas impurity as the current density decreases. Herein, we revised the most promising recent developments in materials, cell design, and system integration aimed at conquering the aforementioned challenges. It is shown that the implementation of advanced components and control strategies, e.g. electrolyte management, is vital to enhance the efficiency at high current densities and expand the load range of operation by maintaining the high gas purity.

Addresses

[1] Institute of Engineering Thermodynamics, German Aerospace Center, Pfaffenwaldring 38-40, Stuttgart 70569, Germany

[2] University of Stuttgart, Faculty 6 – Aerospace Engineering and Geodesy, Stuttgart 70569, Germany

Corresponding author: Corresponding author: Razmjooei, Fatemeh (fatemeh.razmjooei@dlr.de)

[a] These authors have equal authorship contribution.

Current Opinion in Electrochemistry 2024, **47**:101552

This review comes from a themed issue on **Electrochemical Materials and Engineering (2024)**

Edited by **Sangaraju Shanmugam** and **Tao Hang**

For complete overview about the section, refer Electrochemical Materials and Engineering (2024)

Available online 8 June 2024

https://doi.org/10.1016/j.coelec.2024.101552

Introduction

A complete transformation in the energy sector, i.e. energy production, transport, and consumption, holds the key to reduce global CO_2 emissions from around 32 Gt in 2023 to less than 2 Gt in 2050 [1]. The need to reduce greenhouse gas (GHG) emissions has promoted the use of what is called "green H_2," i.e. hydrogen produced by water electrolysis employing renewable power sources [2]. Green H_2 production is expected at first to substitute conventional H_2 produced from fossil sources in the chemical industry, but might then also become a major energy carrier potentially used for long- and short-term energy storage (chemical storage) to balance energy demand and production [3,4]. The high purity H_2 obtained by water electrolysis (>99.9%) can later be used for power generation through thermo-mechanical or electro-chemical convertors, synthetic fuels and other hydrogen derivatives production, and in the chemical industry [5,6]. According to the Net Zero Emissions by 2050 Scenario, rising hydrogen use is expected to reach from 95 Mt in 2022 to more than 660 Mt in 2050, increasing from 0.1% to 60% of the share of electrolysis (3000 GW electrolyzers) [7,8].

Alkaline water electrolysis (AWE) is a mature technology with a high technology readiness level (TRL 9 [9]) and represents 58% of the electrolyzer manufacturing capacity in Europe [10]. Thanks to its cost benefits, AWE presents a promising solution for large-scale hydrogen production [11]. By 2023, there was 81 MW_{el} of installed capacity of AWE and 1200 MW_{el} under construction [10]. Typically, its operation temperature ranges from 40°C to 80°C, and pressures reach up to 30 bar [4,12]. The entire system is designed for lifetimes greater than 60.000 h and high H_2 conversion efficiency, which currently is close to 70% considering the lower heat value of H_2 [3]. The coupling of renewable power energy sources (RES) with H_2 production is theoretically possible thanks to the electrolyzers electrical fast response [5], but historically the AWE systems, including balance of plant (BoP) equipment, have been designed for operation at steady-state conditions [4]. The limitation of current densities upto 0.2–0.6 $A \cdot cm^{-2}$ [13,14] combined with a minimum

partial load of 10%—40% of the nominal load [15], restrict the ability of the AWE system to operate under the highly variable loads associated to RES. Furthermore, the slow thermal dynamic response at system level, which leads operating at lower temperatures to avoid component damage during fast load increase, reduces AWE efficiency. The main challenges identified for the AWEs, particularly when integrated with RES, are the low efficiency, low gas purity at low loads, high cell voltage at high current densities, long-term durability, cost, and the system's dynamic response [3,4,15]. Innovations could demonstrate AWE's potential to increase current density and hydrogen production while simultaneously decreasing costs [11].

In this context, researchers have directed their efforts toward enhancing and optimizing cell/stack material and configuration, adjustment of operation under dynamic, and partial loads for better upstream and downstream AWE integration. This study highlights the latest developments in AWEs technology and its integration into the energy system, with the specific focus on challenges associated with component level and operation under fluctuating load profiles and the prerequisites for downstream integration.

Developments at cell/stack level design and its components

In the following section, cell/stack and material designs for AWE are discussed, along with the most advanced practices. The commonly used stack configuration, series cells electrically connected by bipolar plates, is introduced in Figure 1(**a—c**) [14]. The cell is composed of two half-cells separated by a diaphragm or membrane to minimize the gas mixture, and each half cell includes an electrode, a gas diffusion layer to facilitate the bubble removal, and a bipolar plate. At the cell level, modifications of gap between electrodes, electrolyte, and gas flow inside the cell, electrodes and their microstructures, and separator properties have resulted in an increased durability and efficiency due to a decrease in the overall cell resistance, including ohmic and activation losses. As shown in Figure 1(**d,e**), at lower current densities, the cell performance is governed mainly by the catalytic activity, whereas at higher current densities, the ohmic losses related to separators and electrode microstructure play a major role [16]. In particular, electrodes, their porous transport layer's microstructure, and separator's conductivity impact the ohmic losses associated with mass transport, by affecting the ion transport to the reacting sites, and the bubble removal capacity [11].

Precious metal-based catalysts demonstrated the highest activity for the hydrogen and oxygen evolution reaction (HER, OER). However, due to its scarcity and cost, they have been replaced by Ni-based electrodes. Table 1 summarizes recently developed catalysts for OER and HER. It can be seen that comparison between different catalysts is not straightforward since there is not yet a harmonized protocol among scientific community for the performance characterization. Reviews on promising nonprecious metal catalyst developments such as Fe-(Ni or Co) for OER, transition metal nitrides, and Ni—Mo for HER can be found in Refs. [17,18] and [19].

Unsteady operation of the commonly used Ni-based catalysts can contribute to their deactivation due to microstructural and chemical changes [20]. Anode based on NiFe-hydroxide/oxide-coated stainless steel has shown a stable overpotential after 20,000 potential cycles from 0.5 to 1.8 V (vs. reference hydrogen electrode (RHE), tested at 20 °C in 7 M KOH), while under the same conditions, pure Ni showed a 100 mV increase in overpotentials at 0.1 $A \cdot cm^{-2}$ [20]. Self-repairing catalyst layers have been developed based on cobalt hydroxide nanosheets (Co-ns) with a tripodal ligand on Ni and were able to maintain their low overpotential with an increase of just 9 mV after 40,000 potential cycles (from 0.5 to 1.8 V vs. RHE). The repairing process occurred thanks to the addition of a dispersion of Co-ns to the 1 M KOH electrolyte, which were deposited on the Ni anode during the constant current phases of the test [21]. The durability of the electrodes is also affected by the transients during start-up and shutdown, which generate a reverse current flow during the off periods through the ionic transport provided by the electrolyte in the stack manifold (Figure 1(**b**)) and promote an irreversible oxidation of the Ni cathode to β-$Ni(OH)_2$ or NiO [22]. Efforts to limit this degradation phenomenon include the implementation of cathodic protection systems by sacrificial anodes [22] and the design of electrodes with sacrificial species incorporated into them [23].

The energy losses that arise from the formation of bubbles within electrolysis systems, by blocking the catalyst surface and increasing activation and ohmic loss [24], limit the maximum operating current density [25]. In a recent review on the effect of bubbles on system efficiency, it has been shown that at least 5%—10% of the electrolysis system energy can be saved by mitigating bubble formation and that strategies such as centrifuging the electrolyzer to apply a supergravity environment for a gas bubble-free operation can lead to an increase of 9%—17% of the stack energy efficiency (at current densities greater than 500 $mA \cdot cm^{-2}$ and relative to the higher heating value of hydrogen) [25]. Novel systems, characterized by micro-structured porous electrodes [16] and capillary-fed alkaline electrolysis cells (Figure 1(**f—i**)) [26], hold the promise of a significant leap in energy efficiency thanks to a decrease in bubble accumulation or directly avoiding bubble formation. Studies on the effect of the microstructure of Ni electrodes operated in zero-gap flow-through single cell configuration (Figure 1(**d,e**)) showed the existence of an

Figure 1

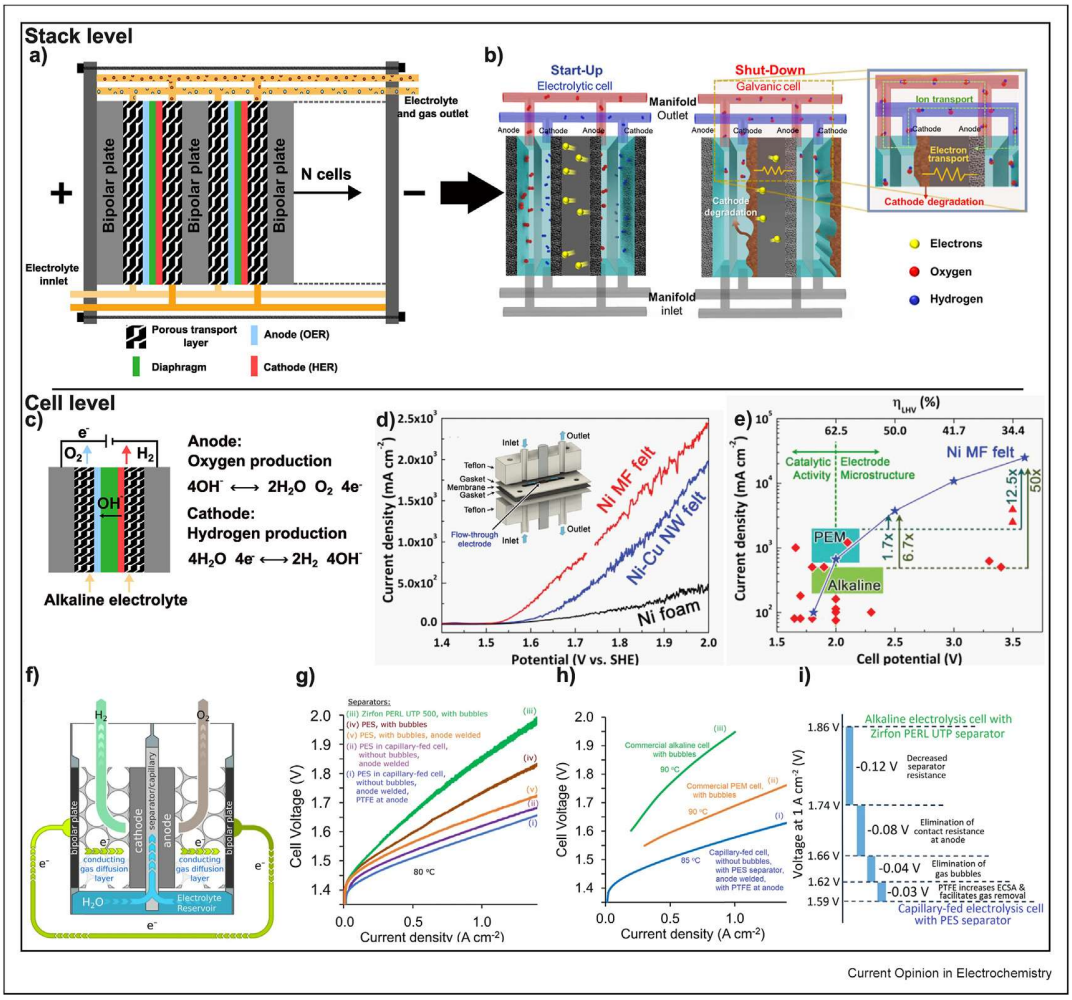

Electrolyzer at stack and cell level. (**a**) Schematic representation of the stack components. (**b**) Degradation mechanisms during shut-down; along with the electrodes, the electrocal circuit is completed by the bipolar plate (e-transport) and the electrolyte present in the stack manifold (ion transport). During operation, each cell acts as an electrolytic cell, but during shut down, a reverse current flow is generated, and the anode and cathode of two adjacent cells reverse their reactions and form a galvanic cell. This leads to the Ni electrode deactivation by the formation of β - $Ni(OH)_2$ or NiO (adapted from Ref. [22]). (**c**) Electrical circuits, and electrochemical reactions at the cell level in alkaline media. (**d**) Effects of changes in the electrode microstructure on the OER potential. The electrodes were tested in a 1 M KOH solution in a flow-through single cell equipped with a reference electrode to measure the anode potential. Three Ni porous electrodes with different surface areas and porosities were tested (ordered by decreasing surface area and increasing bubble removal capability): nanowire felt (Ni NW), microfiber felt (Ni MF), and Ni foam (adapted from Ref. [16]). (**e**) Comparison of the best-performing electrode in Ref. [16] with the state-of-the-art of water electrolysis. Square red symbols represent the maximum current densities for alkaline electrolysis reported in the literature, while the red triangles represent the results for membraneless flow-through alkaline electrolyzers. The shaded areas for AEL and PEM correspond to operating industrial conditions (adapted from Ref. [16]). (**f**) Innovative cell design proposed by Hodges et al., 2022 [26] where the electrolyte is feed by capillarity (achieved with a polyether sulfone (PES) separator), and bubble formation is avoided. (**g**) Comparison of the capillary-fed performance at different configurations with standard cells using Zirfon™ as separator (NiFeOOH as anode and Pt/C as cathode). (**h**) Comparison of the capillary-fed cell performance with commercial alkaline and PEM cells. (**i**) Sources of improved performance in the capillary-fed cell at 1 $A.cm^{-2}$ (**f, g, h,** and **i** adapted from Ref. [26]).

optimal pore size related to the balance between increasing surface area and decreasing bubble removal [16]. They have also shown that different types of electrodes with different structures and porosity can impact reducing the ohmic loss stemmed from the bubble formation and accumulation [16]. Modifications on the separators can also improve their performance at high current densities. Recently, the substitution of porous diaphragms with ion-solvating membranes have resulted in current densities >1.7 $A{\cdot}cm^{-2}$ at 1.8 V combined with a low hydrogen permeability in cells based on Raney Ni-type electrodes immersed in

Table 1

Recent catalyst developments.

Chemistry	Microstructure	Experimental conditions	Overpotential (mV) @ i ($mA.cm^{-2}$)	Stability test duration	Research focus	Ref.
Anodes						
Ru– NiFe	Ru on NiFe defect-rich LDH nanosheets supported on 3D skeleton of Ni foam	O_2 saturated 1 M KOH at 25 °C	220 @ 100	100 h at 100 $mA \cdot cm^{-2}$	Increase catalytic activity by structural and chemical changes	[29]
$Ni_{0.8}Fe_{0.2}$–AHNA	Ultrathin (1–5 nm) and amorphous-anchored NiFe alloy nanowire (core) array	1 M KOH at 25 °C	248 @ 500	120 h	Increase catalytic activity by microstructural changes	[30]
Pt–$Ni(OH)_2$@NM	Nanowire/nanosheet composite structure	1 M KOH	269 @ 100	600 h	Increase catalytic activity by chemical changes	[31]
NiFe-HyOx/Stainless Steel (SS)	SS-anode covered by 850 nm-thick NiFe-hydroxide/oxide-catalyst-layer (comprised of particles-like and nano-scale-pores (3–5 nm in diameter)	7 M KOH at 20 °C.	270 @ 100	20,000 potential cycles of 0.5 and 1.8 V	Overpotential and stability comparison between Ni to NiFe-HyOx/SS anodes	[20]
Mo–NiO@NiFe LDH	NiFe-layered double hydroxide (LDH) nanosheets attached on Mo–NiO microrods	6.7 M KOH at 80 °C	253 @ 1000	1200 h	Increase stability and catalytic activity by microstructural changes	[32]
Ni + Co	Ni wire covered with electrochemically deposited Co nanosheets (ns)	1 M KOH at 80 °C + Co-ns dispersion	360 @100	40,000 cycles (0.5–1.8 V vs RHE)	Increase stability under fluctuating loads by chemical design changes	[21]
$CuCe_{0.5}Co_{1.5}O_x$	Ce-substituted spinel nanoparticles, phase-transfer coprecipitation synthesis method	1 M KOH	294 @ 10	5000 accelerated cyclic voltammetry at 50 $mV \cdot s^{-1}$	Investigate Transition-metal oxides as OER catalysts	[33]
Fe–Ni–Co	Polished metallic surface	1 M NaOH	310 @ 10	50 h	Increase catalytic activity by chemical changes	[34]
Ru– NiFe	Ru on NiFe defect-rich LDH nanosheets supported on 3D skeleton of Ni foam	N_2 saturated 1 M KOH at 25 °C	61 @ 100	100 h at 100 $mA \cdot cm^{-2}$	Changes in the local coordination environments of Ru sites to increase performance	[29]
Pt–$Ni(OH)_2$@NM	Nanowire/nanosheet composite structure	1 M KOH	68 @ 100	600 h	Use PT to improve nickel wire mesh catalytic activity for a low cost and efficient catalyst development	[31]
Ni_3N/Co_2N	Macro porous network structure	1M KOH	70 @100	100 h	Increase catalytic activity by interface engineering	[35]
Ni based cathode alloyed with Mo	Nanostructured (periodic surface structures (LIPSS) Ni mesh by femto-laser treatment	7.3 M KOH at 80 °C	135 @ 100	3 days	Increase catalytic activity by changes in the chemistry and microstructure of the electrode	[36]
Fe-13.37Co-11.37Ni-3.21Cr-1.24Mo-0.22C	3D printed martensitic steel with porous and lamellar structures	1 M KOH at RT	800 @ 500	140 h at 570 $mA \cdot cm^{-2}$ 450 h at 500 $mA \cdot cm^{-2}$	Increase catalytic activity and reduce cost by employing binder free steel electrodes with high active area	[37]

aqueous 24% KOH at 80 °C [27,28]. The stability of such membranes have been improved thanks to a new membrane reinforcement, reaching 1000 h of operation without cell failure [27].

System-level upstream and downstream integration

In the following sections, possible upstream and downstream process integration are presented, including its complexities and recent advances. Figure 2 presents a summary of the integration at a system level.

Transient operation and upstream integration including both experimental and simulation

The integration of RES with hydrogen production can be achieved by implementing on-grid (RES and electrolyzer connected to the grid, blue in Figure 2) or off-grid systems (RES and electrolyzer isolated from the grid, gray in Figure 2). The system integration should consider the characteristics of the RES and optimize the topology of the electrical coupling [38,40], the power allocation strategies [41,42] and the operation of the hydrogen plant. In this review, we will focus on the advances related to the aspect of operation.

The inherent RES fluctuation subjects the connected AWE to fast load changes and a wide load range [43]. The gas impurity is one of the limiting factors in the dynamic operation of AWEs, since it provokes safety shutdowns to prevent the formation of explosive H_2/O_2 mixtures, affecting the stability and power quality of the electrical system [40] and limiting the minimum partial load to 10%–40% of the AWE's nominal power [13,15]. In particular, the lower current densities associated with the partial load will reduce the electrolyzer gas production and consequently reduce the dilution of the impurities, which can result in an unsafe impurity concentration level [4]. The main source of impurity in an AWE is the gas contained in the electrolyte recirculation stream when the system is operated in mixed cycle mode to avoid concertation gradients between the anode and cathode sides [44]. Increasing electrolyte concentration decreases the gas impurity by decreasing gas solubility and diffusion, the upper limit being given by the maximum conductivity achieved by concentrations of 32.5 wt% [44]. Modifications of system operation such as higher temperature operation could improve gas purity in mixed-mode electrolyte circulation by reducing the solubility of the gases and increasing the bubble rise in the electrolyte/gas separators, which is beneficial for the electrolyte/gas separator's efficiency. The operation of a separate electrolyte circuit also allows to obtain safety levels of H_2 in O_2 at current densities as low as 0.05 $A \cdot cm^{-2}$ and pressures of 20 bar [45]. However,

Figure 2

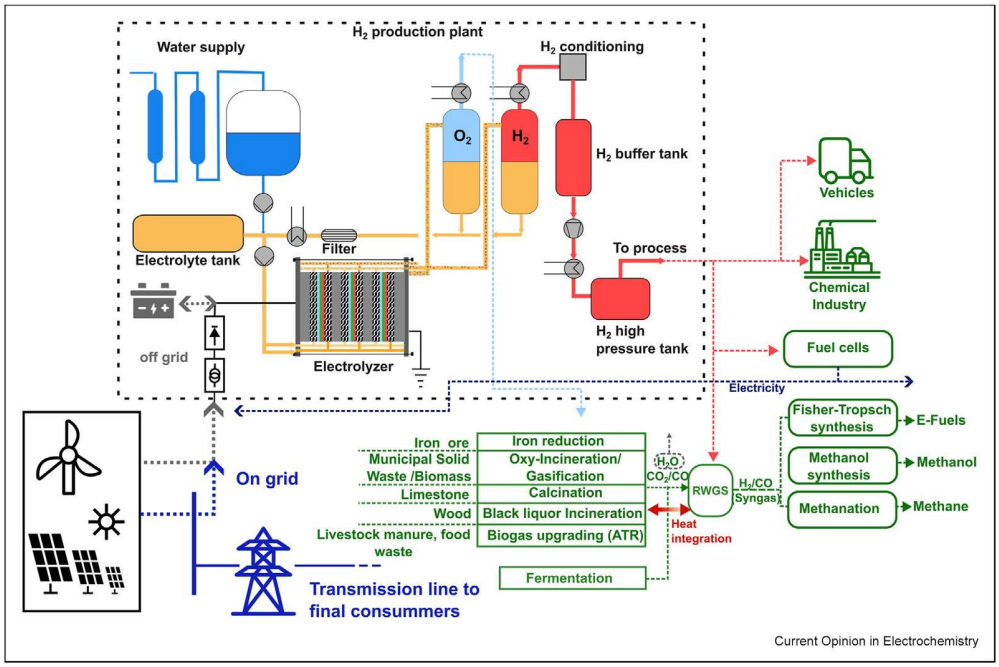

H_2 plant integration into upstream and downstream processes. The boundaries of the H_2 – plant are marked with a doted black rectangle and include: water purification system, electrolyte circuit (tank, pumps, filter), electrolyzer stack, electrolyte/gas separators (for electrolyte/H_2 separation and electrolyte/O_2 separation before the electrolyte is recirculated into the stack) and final H_2 conditioning and pressurization system. The plant can be integrated into the electricity grid (on-grid) or isolated (off-grid). Battery banks and fuel cells can be installed to balance the system. The produced H_2 can be fed to power to gas and power to liquid process, to the chemical industry or transport sector. Image created based on [14,38,39].

temporary mixing of the electrolyte is required to keep the concentration constant. An alternative is the dynamic operation of the electrolytic cycles, which can be achieved by flexible alternation between mixed and separated modes [44]. The operation with adapted electrolyte flow rate depending on the current density was shown to reduce the gas impurity (to a maximum of 1.3% compared to 2.4% of H_2 in O_2 in standard mode) and does not affect the cell voltage when operating a single cell under simulated wind power profiles, as depicted in Figure 3(**a,b**) [43]. Nevertheless, the minimum flow rate for each system should be defined, considering cooling requirements [43] and its effect on the bubble growth rate inside the cell [44]. Simulations have been performed to study the combined effect of dynamic loads and different electrolyte circulation modes (Figure 3(**c,d**)), showing that the dynamic response in terms of impurity accumulation depends on the number of cells and the gas volume of the system [46]. An impressive impurity level below 1 vol% was achieved by designing multiinput multioutput optimal controllers to minimize the pressure difference between the anode and cathode sides in pressurized electrolyzers, under constant pressure separated electrolyte circulation mode, and fluctuating current emulating RES [47].

The fast load changes associated with RES generate potential and temperature variations, resulting in decreased performance and accelerated cell degradation [48]. Electrolyzers coupled to wind power showed a temperature variation of 8°C when using a simple proportional integral differential (PID) control, which limits the temperature set point to 65°C and leads to low operation performance [49]. Recently, temperature controllers based on transient thermal modeling were shown to be fundamental to mitigate the impact of

Figure 3

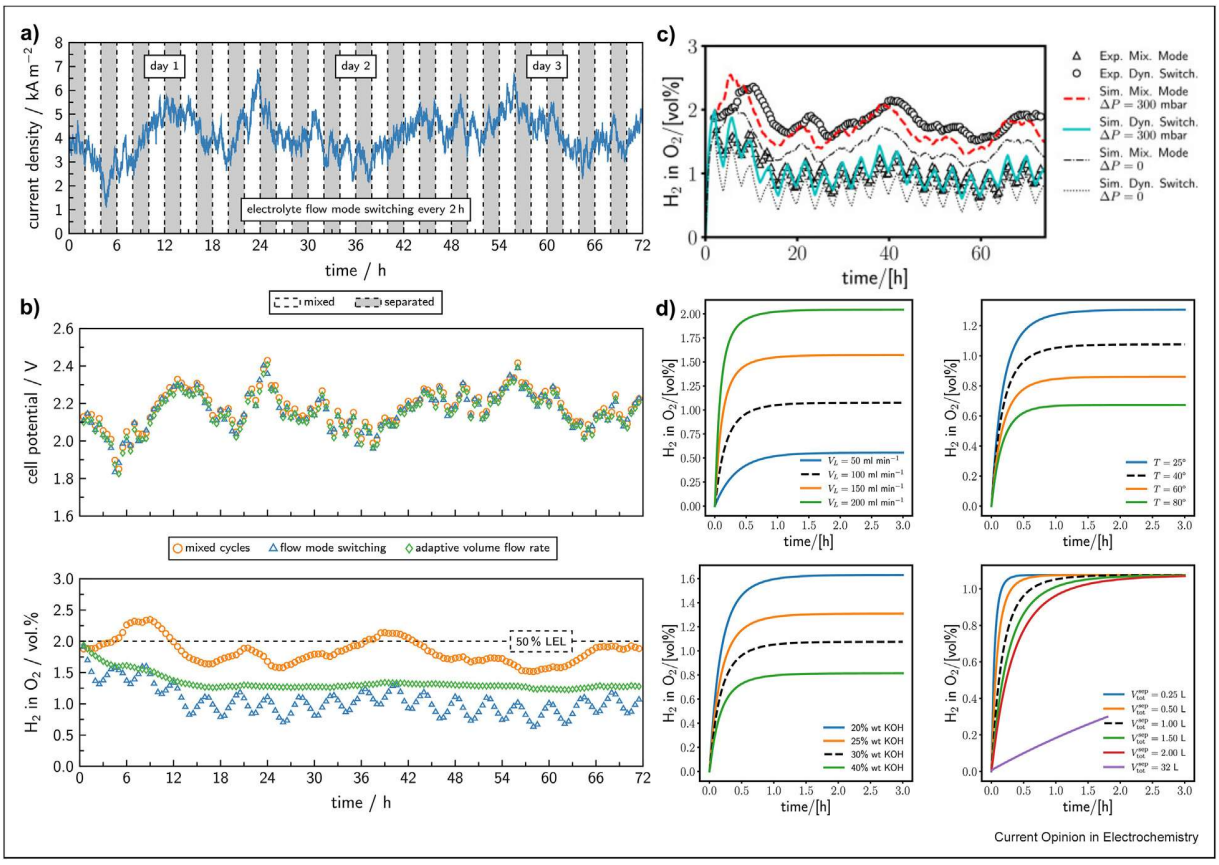

Gas purity control in a single-cell electrolyzer. (**a**) Simulated wind profiles utilized to test different control strategies. The duration of each electrolyte circulation mode is shown for the case of switching from separated to mixed circulation [43]. (**b**) Variation of the cell voltage and gas purity under the simulated wind profile and different electrolyte circulation strategies (mixed mode and fixed volume flow, mixed mode, and variable volume flow, and separated electrolyte circulation) [43]. (**c**) The same data [43] was used to validate a model in Ref. [46], where mixed and alternated circulation modes were simulated. The importance of considering additional gas crossover mechanism caused by a differential pressure between cathode and anode sides was highlighted for near perfect agreement between the model and the experimental results. (**d**) Performing single cell model sensitivity analysis under mixed circulation mode to investigate the dynamic response of the system by varying operation conditions: electrolyte volume flow, temperature, electrolyte concentration, and gas separator volume [46]. Figure adapted from Refs. [43,46].

external disturbances and increase the system efficiency by increasing the temperature set point [50]. Dynamic energy and mass balances could be combined with electrochemical and thermal models to perform sensitivity analyses of changing temperature, mass fraction of KOH in the electrolyte solution and the lye flow rate [51–54], and to develop efficient control strategies.

Researchers have observed that designing a suitable controller for the dynamic operating conditions of AWE systems has been shown to be a powerful tool. It was shown that implementing a multistate transition model (production, stand-by, and off states) led to investigate temperature variations and hydrogen-produced properties, as well as increasing daily revenues [52].

Downstream integration

Figure 2 shows several of the utilization paths of green H_2. Particularly for the mobility sector, chemically stored H_2 in the form of synthetic liquid fuels is considered to be safer and easier to handle than pure H_2. Synthetic liquid fuel production using atmospheric H_2 supply from AWE was simulated and resulted in an energy efficiency of 63.4%. It could be enhanced to 71.5% when system thermal integration was considered [55]. However, for the mobility sector, the overall energy efficiencies reach values close to 21% for E-fuels utilization, while for fuel-cell electric vehicles, this can reach to 31% [53].

High pressures are generally required for downstream integrations, 200–500 bar for hydrogen transport [56], 700 bar for mobility [56], 20–30 bar for reverse water gas shift (RWGS) units and Fischer-Tropsch reactors [57,58]. Figure 4(**a**) shows that the AWE system efficiency, calculated by including the energy consumed to compress hydrogen up to 200 bar, reaches a maximum value in the range of 10–30 bars in the stack. However, further increasing on the stack pressure lead to a decrease of system efficiency. It is also reported that the optimum stack pressure operation could increase with the increase of the final hydrogen compression pressure [59]. It has been reported that incorporating pressurized electrolyzers will contribute to decrease the system cost by reducing the energy consumed for compression [56]. However, pressurization impacts electrolysis energy consumption (as depicted in Figure 4(**b**)) [60] and increases hydrogen crossover [61]. Moreover, the combination of low current densities with high pressure was shown to exacerbate the unfavorable conditions regarding the gas purity [62]. Strategies using separated electrolyte mode and advanced controllers that minimize the gas crossover could pave the way for the operation at higher pressure under fluctuating loads [47]. New materials have been tested in short stacks reaching up to 100 bar [63], but still more advances are necessary to improve durability and gas purity in a wider load range.

Conclusion

The most recent advances in AWE cell, stack, and system levels were reviewed in this short article. Developing new cell/stack components and cell designs with a high bubble removal rate was shown to be a promising strategy to increase efficiency at high current densities. Furthermore, the need of advanced system operational strategies under transient states for upstream integration and the high pressures required for downstream processes were emphasized. The implementation of advanced control systems for the power supply system's temperature and pressure, and using adaptive electrolyte flow rate and concentration could decrease AWE's minimum load, improve its dynamic response when combined with RES, and increase system efficiency. The downstream integration of highly

Figure 4

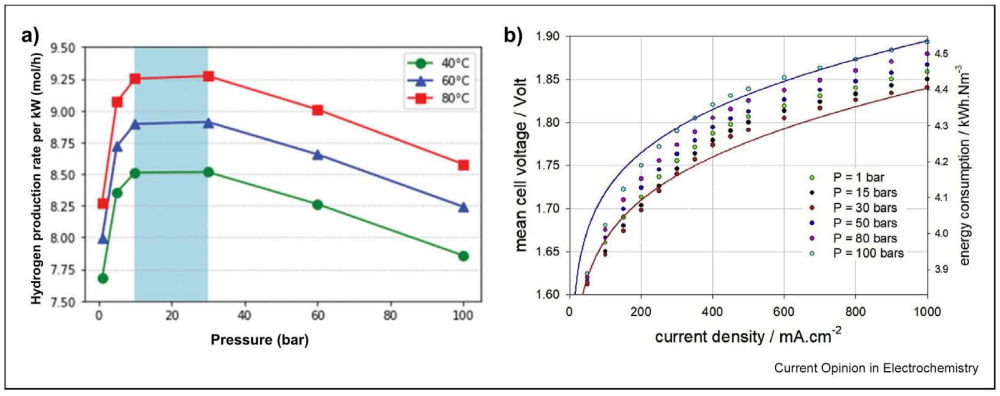

(**a**) Effect of pressure on the hydrogen production efficiency when the energy required for compression up to 200 bar is considered. Results obtained by simulations for an AWE system operating at 0.4 A·cm^{-2} [59]. (**b**) Mean cell voltage variation and energy consumption measured in a 5 cells short stack using optimized electrodes and separators. The experimental results showed an increase in the cell voltage at increasing pressures above 30 bar [63].

pressurized AWE to produce hydrogen, could also increase the overall system efficiency and decrease the system cost by reducing the energy consumed for compression.

Declaration of competing interest

The authors declare that they have no known competing financial interests or personal relationships that could have appeared to influence the work reported in this paper.

Data availability

No data were used for the research described in the article.

References

Papers of particular interest, published within the period of review, have been highlighted as:

* of special interest
** of outstanding interest

1. IEA: *Net zero by 2050: a roadmap for the global energy sector*. International Energy Agency; 2021.
2. Corengia M, Torres AI: **Coupling time varying power sources to production of green-hydrogen: a superstructure based approach for technology selection and optimal design.** *Chem Eng Res Des* 2022, **183**:235–249, https://doi.org/10.1016/j.cherd.2022.05.007.
3. Carmo M, Stolten D: **Energy storage using hydrogen produced from excess renewable electricity**. In *Science and engineering of hydrogen-based energy technologies*; 2019:165–199, https://doi.org/10.1016/b978-0-12-814251-6.00004-6.
4. Brauns J, Turek T: **Alkaline water electrolysis powered by renewable energy: a review processes.** *Processes* 2020, **8**:248, https://doi.org/10.3390/pr8020248.
5. Eichman J, K.H, Peters M: *Novel electrolyzer applications: providing more than just hydrogen*. National Renewable Energy Laboratory; 2014.
6. Ursua A, Gandia LM, Sanchis P: **Hydrogen production from water electrolysis: current status and future trends.** *Proc IEEE* 2012, **100**:410–426, https://doi.org/10.1109/jproc.2011.2156750.
7. Hydrogen Council, M.C: *Hydrogen for net-zero – a critical cost-competitive energy vector*. 2021.
8. IEA: *Global hydrogen review 2023*. International Energy Agency; 2023.
9. IEA. 2023 05.10.2023]; Available from: https://www.iea.org/energy-system/low-emission-fuels/electrolysers.
10. Fonseca J, Muron M, Pawelec G, Petar Yovchev I, Bellomo N, Muse K, Kuhn M, Fraile D, Waciega K, Azzimonti M, Brodier C, Alcalde I, Antal MI, Marsili L, Pafiti A, Espitalier-Noël M, Giusti N, Durdevic D. In *Clean hydrogen monitor 2023*. Edited by Michela Bortolotti PC, Timmermans M; 2023. Hydrogen Europe.
11. Emam AS, Hamdan MO, Abu-Nabah BA, Elnajjar E: **A review on recent trends, challenges, and innovations in alkaline water electrolysis.** *Int J Hydrogen Energy* 2024, **64**:599–625, https://doi.org/10.1016/j.ijhydene.2024.03.238.
12. Ansar AS, Gago AS, Razmjooei F, Reißner R, Xu Z, Friedrich KA: **Alkaline electrolysis – status and prospects**. In *Electrochemical power sources: fundamentals, systems, and applications*; 2022:165–198, https://doi.org/10.1016/b978-0-12-819424-9.00004-5.
13. de Groot MT, Kraakman J, Garcia Barros RL: **Optimal operating parameters for advanced alkaline water electrolysis.** *Int J Hydrogen Energy* 2022, **47**:34773–34783, https://doi.org/10.1016/j.ijhydene.2022.08.075.
14. International Renewable Energy Agency: *Green hydrogen cost reduction: scaling up electrolysers to meet the 1.5°C climate goal*. Abu Dhabi: IRENA; 2020.
15. Stolten JMaD: **Challenges in water electrolysis and its development potential as a key technology for renewable energies**. In *ECS Meeting Abstracts*; 2012.
16. * Yang F, Kim MJ, Brown M, Wiley BJ: **Alkaline water electrolysis at 25 A cm^{-2} with a microfibrous flow-through electrode.** *Adv Energy Mater* 2020, **10**, https://doi.org/10.1002/aenm.202001174.
Testing electrodes with different porosities in a flow-through AWE cell, the authors demonstrated that there is a balance between decreasing pore size to obtain a higher surface area and increasing it to facilitate bubble removal. Using electrodes made of Ni microfiber felt, they were able to operate the cell for more than 100 h at an outstanding high current density (25 Acm-2)
17. Anantharaj S, Kundu S, Noda S: **"The Fe effect": a review unveiling the critical roles of Fe in enhancing OER activity of Ni and Co based catalysts.** *Nano Energy* 2021:80, https://doi.org/10.1016/j.nanoen.2020.105514.
18. Tang S, Zhang Z, Xiang J, Yang X, Shen X, Song F: **Recent advances in transition metal nitrides for hydrogen electrocatalysis in alkaline media: from catalyst design to application.** *Front Chem* 2022, **10**, 1073175, https://doi.org/10.3389/fchem.2022.1073175.
19. Park SH, To DT, Myung NV: **A review of nickel-molybdenum based hydrogen evolution electrocatalysts from theory to experiment.** *Appl Catal Gen* 2023:651, https://doi.org/10.1016/j.apcata.2022.119013.
20. Todoroki N, Wadayama T: **Electrochemical stability of stainless-steel-made anode for alkaline water electrolysis: surface catalyst nanostructures and oxygen evolution overpotentials under applying potential cycle loading.** *Electrochem Commun* 2021, **122**, https://doi.org/10.1016/j.elecom.2020.106902.
21. Kuroda Y, Nishimoto T, Mitsushima S: **Self-repairing hybrid nanosheet anode catalysts for alkaline water electrolysis connected with fluctuating renewable energy.** *Electrochim Acta* 2019, **323**, https://doi.org/10.1016/j.electacta.2019.134812.
22. Kim Y, Jung SM, Kim KS, Kim HY, Kwon J, Lee J, Cho HS, Kim YT: **Cathodic protection system against a reverse-current after shut-down in zero-gap alkaline water electrolysis.** *JACS Au* 2022, **2**:2491–2500, https://doi.org/10.1021/jacsau.2c00314.
23. * Kim Ik-Sun, Kim MinJoong, Oh Hyun-Jung, Lee Sang-Yeon, Lee Yong-Kul, Lee Changsoo, Lee Jae Hun, Cho Won Chul, Kim Sang-Kyung, Joo Jong Hoon, Kim Chang-Hee: **Sacrificial species approach to designing robust transition metal phosphide cathodes for alkaline water electrolysis in discontinuous operation.** *J Mater Chem A* 2021, **9**:16713–16724, https://doi.org/10.1039/D1TA01181B.
The authors studied the degradation mechanisms of a CoPx cathode under off periods, which are frequent during intermittent operation. It was reported that the irreversible formation of oxide and hydroxide was responsible for the activity degradation. The co-deposition of Mn as a sacrificial species reduced the activity loss during hold-off periods, being a promising alternative to limit the electrode degradation when AWE electrolyzers are coupled with renewable power sources.
24. Niblett D, Delpisheh M, Ramakrishnan S, Mamlouk M: **Review of next generation hydrogen production from offshore wind using water electrolysis.** *J Power Sources* 2024:592, https://doi.org/10.1016/j.jpowsour.2023.233904.
25. Swiegers GF, Terrett RNL, Tsekouras G, Tsuzuki T, Pace RJ, Stranger R: **The prospects of developing a highly energy-efficient water electrolyser by eliminating or mitigating bubble effects.** *Sustain Energy Fuels* 2021, **5**:1280–1310, https://doi.org/10.1039/d0se01886d.
26. ** Hodges A, Hoang AL, Tsekouras G, Wagner K, Lee CY, Swiegers GF, Wallace GG: **A high-performance capillary-fed electrolysis cell promises more cost-competitive renewable hydrogen.** *Nat Commun* 2022, **13**:1304, https://doi.org/10.1038/s41467-022-28953-x.

The authors proposed a new electrolysis cell architecture, which results in a simplified balance of plant. The new design contributes to solve two problems: the increased ohmic loss at high current densities (by avoiding bubble formation) and the limited partial load range (by minimizing gas cross over)

27. * Trisno MLA, Dayan A, Lee SJ, Egert F, Gerle M, Kraglund MR, Jensen JO, Aili D, Roznowska A, Michalak A, Park HS, Razmjooei F, Ansar S-A, Henkensmeier D: **Reinforced gel-state polybenzimidazole hydrogen separators for alkaline water electrolysis.** *Energy Environ Sci* 2022, **15**:4362–4375, https://doi.org/10.1039/d2ee01922a.

The research work focuses in the development of alternative separators that enable higher current densities by reducing Ohmic losses. The authors developed a reinforced polybenzimidazole (PBI) membrane, which combines the high conductivity of previous PBI membranes with a higher durability, with performance comparable to PEM cells but utilizing noble metal-free electrodes. Furthermore, it was shown that the produced ion-solvating membrane has low hydrogen permeability, making it a promising separator to work at low differential pressures.

28. Kraglund MR, Carmo M, Schiller G, Ansar SA, Aili D, Christensen E, Jensen JO: **Ion-solvating membranes as a new approach towards high rate alkaline electrolyzers.** *Energy Environ Sci* 2019, **12**:3313–3318, https://doi.org/10.1039/c9ee00832b.

29. Zhai P, Xia M, Wu Y, Zhang G, Gao J, Zhang B, Cao S, Zhang Y, Li Z, Fan Z, Wang C, Zhang X, Miller JT, Sun L, Hou J: **Engineering single-atomic ruthenium catalytic sites on defective nickel-iron layered double hydroxide for overall water splitting.** *Nat Commun* 2021, **12**:4587, https://doi.org/10.1038/s41467-021-24828-9.

30. Liang C, Zou P, Nairan A, Zhang Y, Liu J, Liu K, Hu S, Kang F, Fan HJ, Yang C: **Exceptional performance of hierarchical Ni–Fe oxyhydroxide@NiFe alloy nanowire array electrocatalysts for large current density water splitting.** *Energy Environ Sci* 2020, **13**:86–95, https://doi.org/10.1039/c9ee02388g.

31. Zhang J, Dang J, Zhu X, Ma J, Ouyang M, Yang F: **Ultra-low Pt-loaded catalyst based on nickel mesh for boosting alkaline water electrolysis.** *Appl Catal B Environ* 2023:325, https://doi.org/10.1016/j.apcatb.2022.122296.

32. Ye J, Yuan B, Peng W, Liang J, Han Q, Hu R: **Highly stable MoNiO@NiFe-layered double hydroxide heterojunction anode catalyst for alkaline electrolyzers with porous membrane.** *ACS Appl Mater Interfaces* 2024, https://doi.org/10.1021/acsami.4c00974.

33. Shi W, Zhang Y, Bo L, Guan X, Wang Y, Tong J: **Ce-substituted spinel CuCo(2)O(4) quantum dots with high oxygen vacancies and greatly improved electrocatalytic activity for oxygen evolution reaction.** *Inorg Chem* 2021, **60**:19136–19144, https://doi.org/10.1021/acs.inorgchem.1c02931.

34. Le Formal F, Yerly L, Potapova Mensi E, Pereira Da Costa X, Boudoire F, Guijarro N, Spodaryk M, Züttel A, Sivula K: **Influence of composition on performance in metallic iron–nickel–cobalt ternary anodes for alkaline water electrolysis.** *ACS Catal* 2020, **10**:12139–12147, https://doi.org/10.1021/acscatal.0c03523.

35. Song F, Zhang T, Zhou D, Sun P, Lu Z, Bian H, Dang J, Gao H, Qian Y, Li W, Jiang N, Dummer H, Shaw JG, Chen S, Chen G, Sun Y, Rao Y: **Charge transfer of interfacial catalysts for hydrogen energy.** *ACS Mater Lett* 2022, **4**:967–977, https://doi.org/10.1021/acsmaterialslett.2c00143.

36. Hoffmann V, Hoffmann L, Schade W, Turek T, Gimpel T: **Femtosecond laser molybdenum alloyed and enlarged nickel surfaces for the hydrogen evolution reaction in alkaline water electrolysis.** *Int J Hydrogen Energy* 2022, **47**:20729–20740, https://doi.org/10.1016/j.ijhydene.2022.04.194.

37. Zhou P, Niu P, Liu J, Zhang N, Bai H, Chen M, Feng J, Liu D, Wang L, Chen S, Kwok CT, Tang Y, Li R, Wang S, Pan H: **Anodized steel: the most promising bifunctional electrocatalyst for alkaline water electrolysis in industry.** *Adv Funct Mater* 2022, **32**, https://doi.org/10.1002/adfm.202202068.

38. Zhao W, Nielsen MR, Kjær M, Iov F, Nielsen SM: **Grid integration of a 500 kW alkaline electrolyzer system for harmonic analysis and robust control**. *e-Prime Adv Electr Eng Electr Energy* 2023:5, https://doi.org/10.1016/j.prime.2023.100217.

39. Ostadi M, Paso KG, Rodriguez-Fabia S, Øi LE, Manenti F, Hillestad M: **Process integration of green hydrogen: decarbonization of chemical industries.** *Energies* 2020, **13**, https://doi.org/10.3390/en13184859.

40. Xia Y, Cheng H, He H, Wei W: **Efficiency and consistency enhancement for alkaline electrolyzers driven by renewable energy sources.** *Commun Eng* 2023, **2**, https://doi.org/10.1038/s44172-023-00070-7.

41. Becker M, Brauns J, Turek T: **Battery-buffered alkaline water electrolysis powered by photovoltaics.** *Chem Ing Tech* 2021, **93**:655–663, https://doi.org/10.1002/cite.202000151.

42. Zhao YY, Zhu ZZ, Tang SH, Guo YJ, Sun HX: **Electrolyzer array alternate control strategy considering wind power prediction.** *Energy Rep* 2022, **8**:223–232, https://doi.org/10.1016/j.egyr.2022.08.169.

43. Brauns J, Turek T: **Experimental evaluation of dynamic operating concepts for alkaline water electrolyzers powered by renewable energy.** *Electrochim Acta* 2022, **404**, https://doi.org/10.1016/j.electacta.2021.139715.

44. Haug P, Koj M, Turek T: **Influence of process conditions on gas purity in alkaline water electrolysis.** *Int J Hydrogen Energy* 2017, **42**:9406–9418, https://doi.org/10.1016/j.ijhydene.2016.12.111.

45. Trinke P, P.H, Brauns J, Bensmann B, Hanke-Rauschenbach R, Turek T: **Hydrogen crossover in PEM and alkaline water electrolysis: mechanisms, direct comparison and mitigation strategies.** *J Electrochem Soc* 2018, **165**:F502–F513, https://doi.org/10.1149/2.0541807jes.

46. Oikonomidis S, Ramdin M, Moultos OA, Bos A, Vlugt TJH, Rahbari A: **Transient modelling of a multi-cell alkaline electrolyzer for gas crossover and safe system operation.** *Int J Hydrogen Energy* 2023, **48**:34210–34228, https://doi.org/10.1016/j.ijhydene.2023.05.184.

47. David M, Bianchi F, Ocampo-Martinez C, Sánchez-Peña R: **H2 purity control of high-pressure alkaline electrolyzers.** *IFAC PapersOnLine* 2021, **54**:109–114, https://doi.org/10.1016/j.ifacol.2021.08.227.

48. Kojima H, Nagasawa K, Todoroki N, Ito Y, Matsui T, Nakajima R: **Influence of renewable energy power fluctuations on water electrolysis for green hydrogen production.** *Int J Hydrogen Energy* 2023, **48**:4572–4593, https://doi.org/10.1016/j.ijhydene.2022.11.018.

49. Ren ZB, Wang JY, Yu ZY, Zhang C, Gao SW, Wang PJ: **Experimental studies and modeling of a 250-kW alkaline water electrolyzer for hydrogen production.** *J Power Sources* 2022, **544**, https://doi.org/10.1016/j.jpowsour.2022.231886.

50. Qi R, Li J, Lin J, Song Y, Wang J, Cui Q, Qiu Y, Tang M, Wang J: **Thermal modeling and controller design of an alkaline electrolysis system under dynamic operating conditions.** *Appl Energy* 2023:332, https://doi.org/10.1016/j.apenergy.2022.120551.

51. Sakas G, Ibáñez-Rioja A, Ruuskanen V, Kosonen A, Ahola J, Bergmann O: **Dynamic energy and mass balance model for an industrial alkaline water electrolyzer plant process.** *Int J Hydrogen Energy* 2022, **47**:4328–4345, https://doi.org/10.1016/j.ijhydene.2021.11.126.

52. * Zheng Y, You S, Bindner HW, Münster M: **Optimal day-ahead dispatch of an alkaline electrolyser system concerning thermal–electric properties and state-transitional dynamics.** *Appl Energy* 2022:307, https://doi.org/10.1016/j.apenergy.2021.118091.

In this study, the authors designed a controller for AWE dynamic operation, considering both electric and thermal aspects. The controller designed was based on coupling several aspects such as state transitions, efficiency, and temperature. The multistate transition model (production, stand-by, and off states) along with their interstates (cold/hot-starts, stand by and shut-down) were adopted.

53. Lee RP, Seidl LG, Meyer B: **Chemical storage of hydrogen in synthetic liquid fuels: building block for CO2-neutral mobility.** *Clean Energy* 2021, **5**:180–186, https://doi.org/10.1093/ce/zkab002.

54. Li Y, Zhang T, Deng X, Liu B, Ma J, Yang F, Ouyang M: **Active pressure and flow rate control of alkaline water electrolyzer based on wind power prediction and 100% energy utilization in off-grid wind-hydrogen coupling system.** *Appl Energy* 2022: 328, https://doi.org/10.1016/j.apenergy.2022.120172.

55. Marchese M, Giglio E, Santarelli M, Lanzini A: **Energy performance of Power-to-Liquid applications integrating biogas upgrading, reverse water gas shift, solid oxide electrolysis and Fischer-Tropsch technologies.** *Energy Convers Manag X* 2020:6, https://doi.org/10.1016/j.ecmx.2020.100041.

56. * Jang D, Cho H-S, Kang S: **Numerical modeling and analysis of the effect of pressure on the performance of an alkaline water electrolysis system.** *Appl Energy* 2021:287, https://doi.org/10.1016/j.apenergy.2021.116554.

Based on a system-level simulation, an AWE system analysis was conducted to study the effect of the operating pressure, from atmospheric to 100 bar, on different parameters like reversible cell voltage, activation and overvoltage, BOP power consumption, and stack performance with an interest in bubble accumulation within. Results revealed that an increase in system efficiency occurs mainly in the range from 1 to 10 bar, while the H2 purity continues to increase up to 20 bar.

57. Adelung S, Maier S, Dietrich R-U: **Impact of the reverse water-gas shift operating conditions on the Power-to-Liquid process efficiency.** *Sustain Energy Technol Assessments* 2021:43, https://doi.org/10.1016/j.seta.2020.100897.

58. Vázquez FV, Koponen J, Ruuskanen V, Bajamundi C, Kosonen A, Simell P, Ahola J, Frilund C, Elfving J, Reinikainen M, Heikkinen N, Kauppinen J, Piermartini P: **Power-to-X technology using renewable electricity and carbon dioxide from ambient air: SOLETAIR proof-of-concept and improved process concept.** *J CO2 Util* 2018, **28**:235–246, https://doi.org/10.1016/j.jcou.2018.09.026.

59. ** Shin Y, Oh J, Shin D: **Analysis of the total energy consumption through hydrogen compression for the operating pressure optimization of an alkaline water electrolysis system.** *Kor J Chem Eng* 2023, **40**:2800–2814, https://doi.org/10.1007/s11814-023-1540-x.

Uncommonly, linking hydrogen production's operating pressure to the product compression needed for mobility and transportation was considered in this study. The authors studied the optimal operating pressure of the electrolyzer according to the compression pressure needed. Different ways of minimizing the operating costs and maximizing the energy efficiency were considered.

60. Ehlers JC, Feidenhans'l AA, Therkildsen KT, Larrazábal GO: **Affordable green hydrogen from alkaline water electrolysis: key research needs from an industrial perspective.** *ACS Energy Lett* 2023, **8**:1502–1509, https://doi.org/10.1021/acsenergylett.2c02897.

61. Lohmann-Richters FP, Renz S, Lehnert W, Müller M, Carmo M: **Review – challenges and opportunities for increased current density in alkaline electrolysis by increasing the operating temperature.** *J Electrochem Soc* 2021, **168**, https://doi.org/10.1149/1945-7111/ac34cc.

62. Brauns J, Turek T: **Model-based analysis and optimization of pressurized alkaline water electrolysis powered by renewable energy.** *J Electrochem Soc* 2023, **170**, 064510, https://doi.org/10.1149/1945-7111/acd9f1.

63. ** Kuleshov NV, Kuleshov VN, Dovbysh SA, Grigoriev SA, Kurochkin SV, Millet P: **Development and performances of a 0.5 kW high-pressure alkaline water electrolyser.** *Int J Hydrogen Energy* 2019, **44**:29441–29449, https://doi.org/10.1016/j.ijhydene.2019.05.044.

A rare high-pressure, up to 100 bar, AWE short-stack of 0.5 kW was tested in this study. Investigations showed that improved and optimized electrodes with a porous catalytic structure and a proper designed diaphragm should be opted for in order to deal with such a pressure. The authors stated that durability reached 1000 h with a limited degradation rate.